2024 IEEE/RSJ International Conference on Intelligent Robots and Systems (IROS)
October 14-18, 2024. Abu Dhabi, UAE

Tightly Coupled Passive UWB Localization for Low-density Anchor Networks

Nushen M. Senevirathna, Oscar De Silva, George K. I. Mann, and Raymond G. Gosine [1]
Faculty of Engineering and Applied Science
Memorial University of Newfoundland

***Abstract*— This study investigates the effectiveness of a passive tightly coupled ultra-wideband (UWB) based inertial navigation system for indoor positioning of mobile platforms. Unlike conventional methods that rely on time difference of arrival (TDOA) or two-way ranging (TWR) measurements, the proposed approach utilizes local reception timestamps directly. An error state Kalman filter with right quaternion error definition is used in the state estimation process. Evaluation is performed first in a Matlab simulation environment and then, using a dataset acquired by flying a quadcopter while monitored by a motion capture system. Timestamp measurements were acquired using custom firmware flashed onto Decawave DWM 1000-DEV hardware. Our findings demonstrate that the proposed system outperforms traditional TDOA methods, providing accurate measurements even in the presence of communication interruptions, with as few as one anchor.**

I. Introduction

Precise localization in global navigation satellite system (GNSS) denied environments such as indoor and urban environments has been a challenging research topic in the recent past. Although visual, inertial, and LIDAR-based systems demonstrate precision over short distances, they are prone to inherent drift due to the integration of stochastic processes[1]. Although GNSS can provide an absolute position measurement to mitigate the drift in outdoor applications, there is no such trivial measurement available in indoor environments. To address this issue, various supplementary localization methods have been proposed incorporating absolute measurements.

UWB based systems provide absolute range measurements relative to a fixed point in the environment, which can be used for drift free localization. When compared to the ranges being measured, UWB timestamp measurements contain a high amount of noise. Due to this reason, UWB measurements alone are usually insufficient for precise positioning. Hence, most precision systems use UWB measurements in combination with visual, LIDAR, or inertial sensors [2].

UWB localization can be broadly categorized into active ranging methods and passive methods. Active ranging methods use two-way time of flight (TOF) to calculate the ranges, which require both the stationary anchor and the localizing node to transmit messages. Improved methods use additional messages to estimate and compensate for the relative clock rate between the transmitter and the receiver [3, 4]. Although active methods generally provide better accuracies and are simpler [5], they have limitations in scalability. On the other hand, passive methods use only one-way TOF information where the localization node generally doesn't need to transmit. These methods can passively localize an arbitrary number of nodes, which is analogous to GNSS. Since the localization node does not need to transmit, in passive systems, the network is unaware of the tags in the vicinity. This is an additional benefit from a privacy and security standpoint [6].

A key challenge of passive UWB indoor localization systems is obtaining a position solution from the timestamp measurements. This is particularly challenging as the arrival timestamp measurements of the mobile node are coupled with its relative position as well as its clock dynamics. Due to these coupled dynamics and imprecise clocks found in the low-cost hardware, achieving time synchronization between the network and the mobile node to the required precision is challenging. In order to circumvent this issue, most of the passive systems use TDOA measurements [7]–[10]. Due to the canceled phase offset in these measurements, the synchronization requirement with the network clock can be eliminated.

However, to obtain TDOA measurements, the transmission gap should be subtracted from the arrival time difference. This, in turn, introduces an error due to the differences between the clocks used for measuring the arrival time difference and the transmission gap. Usually, a first-order correction is applied using an estimated relative clock rate. This estimate can be from a simple low pass filtered clock offset ratio measurement or from a coupled relative clock rate state included in the estimator [10]. However, in scenarios where the transmission gap is substantial, such as in large-scale networks, in low-power applications, or when the network adheres to a transmission schedule, a first-order correction can be insufficient.

A higher level of correction can be achieved by modelling and tracking the variations of clocks. Our previous work [11] uses a separate Kalman filter to keep track of the relative clock rate and its derivative, neglecting the movement dynamics. Although the clock dynamics are modelled, the coupled interactions between the position and the timestamps are neglected in the clock tracking filter. Accuracy and robustness can be further increased by correctly modelling

*This work was supported by the Natural Sciences and Engineering Research Council of Canada and Memorial University of Newfoundland.
Authors are with Memorial University of Newfoundland, Canada.
[1] msenevirathn, oscar.desilva, gmann, rgosine@mun.ca

the coupled interactions between movement dynamics and clock dynamics.

To establish the terminology used, we will refer to the GNSS assisted inertial navigation solutions. A loosely coupled GPS-INS system will use position measurements from a GNSS solution fused with inertial sensor measurements, where the information from the localization solution is generally not used in GNSS solution. A tightly coupled system will use estimated pseudo-ranges and Doppler shift measurements from the GNSS receiver in combination with inertial measurements to obtain a position solution [12, 13]. Whereas an ultra tightly coupled system would utilize navigation filter solutions in carrier phase tracking, resulting in superior results[14, 15]. In these systems, localization information estimated from the navigation filter is used to remove dynamics from the GNSS signal, resulting in improved noise figures.

Following a similar terminology of GNSS systems, a loosely coupled UWB system can be referred as a system that uses a trilateration position solution from UWB measurements in combination with other sensor data [16]. A tightly coupled system would use range measurements or TDOA measurements with or without clock offset ratio measurements, to update a localization solution, usually driven by an inertial odometry [17]–[19]. A system where the receiver tracks the transmitter's clock phase and uses timestamps to correct the localization solution can also be considered as a tightly coupled system, although the coupled interactions are deeper. Due to the coupled dynamics of relative clocks and relative position, these systems enable precise range information with minimal latency. To the best of our knowledge, there has been no work reported that involves passive continuous phase tracking for tightly coupled UWB localization.

As an alternative to passive TDOA localization, we propose tightly coupled time of arrival () passive localization. This method is shown to have improved accuracy and consistency over the traditional TDOA method, while retaining the advantages of passive localization. This method is also capable of holding up well when momentary loss of connection with anchors are present. While the TDOA method requires a minimum of two anchors to obtain a measurement, the proposed method can work even when the connection is dropped down to a single anchor.

To the best of the author's knowledge, this is the first time a tightly coupled system with continuous clock phase tracking has been proposed for UWB localization. Our contributions include; a comparison between TC-TOA and TDOA methods in simulations, and experimental evaluation of the proposed method

II. Methodology

The UWB network is composed of multiple stationary nodes, referred to as anchors. These anchors are in synchronization with each other and transmit periodically. These messages being transmitted include the location of the transmitter in reference to a global coordinate system, as well as the transmission timestamps in reference to a network clock denoted by N. The passive localization problem is defined as how a mobile node L, referred to as a tag, achieves synchronization and solves for its location by listening to the periodic transmissions from the network anchors.

A. Relative clock dynamics

The third-order linear clock model [10] expresses the value of a clock as a third-order linear function of time. We are interested in the value of a clock at an event, particularly transmission tx and reception rx events. We express the value of a local clock L at event ϵ, as $t_L[\epsilon]$.

The relative rate of the mobile node clock L with respect to the network clock N is expressed as,

$$\dot{t}_L^N[\epsilon] = \frac{dt_L}{dt_N}[\epsilon] \tag{1}$$

and the relative clock acceleration as,

$$\ddot{t}_L^N[\epsilon] = \frac{d^2 t_L}{{dt_N}^2}[\epsilon] \tag{2}$$

Since we are interested in tracking the variation of the clock of a mobile node L compared to the UWB network clock, N superscript here should be referred to the network clock. The system is expected to be driven by the noise injected at the third derivative of the clock phase.

$$\dddot{t}_L^N[\epsilon] = \nu_c(dt) \tag{3}$$

where $\nu_c(dt) \sim N(0, \sigma_c^2)$ is the Gaussian noise driving the system [10], which depends on the sampling time dt.

Following the third-order linear model, the relative clock phase is expected to propagate between two events ϵ_k and ϵ_{k+1} according to the following Taylor expansion.

$$t_L[\epsilon_k] = t_L[\epsilon_{k-1}] + \dot{t}_L^N[\epsilon_{k-1}]dt_N + \frac{1}{2}\ddot{t}_L^N[\epsilon_{k-1}](dt_N)^2 + \nu_t(dt_N) \tag{4}$$

where $\nu_t(dt_N) \sim N(0, \sigma_c^2 dt_N^6/20)$ is the integrated Gaussian noise of clock dynamics injected through the third derivative. Furthermore, $\nu_t(dt_N)$ term is expected to capture any residual contributions from higher order terms. dt_N is the time elapsed between the events measured with respect to the network clock.

$$dt_N = t_N[\epsilon_k] - t_N[\epsilon_{k-1}] \tag{5}$$

When referring to the network clock, we will drop the subscript N for simplicity where applicable.

Following the equation (4), considering a single local clock, we introduce the following parameterization for simplification.

$$t[\epsilon_k] = t_0[k-1] + d_1[k-1]\,dt + \frac{1}{2}d_2[k-1]\,dt^2 + \nu_t(dt) \tag{6}$$

Where $t_0[k-1]$ is the value of local clock at the previous synchronization event, and $d_1[k-1]$ and $d_2[k-1]$ are the corresponding parameters related to first and second derivatives

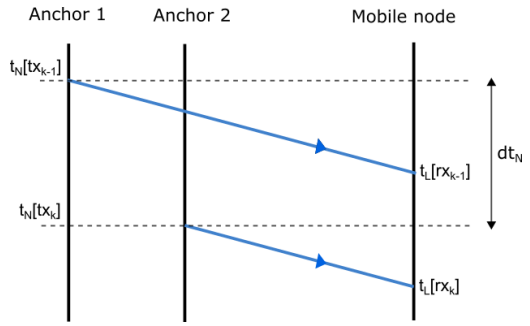

Fig. 1. Message timestamps.

of relative clock phase. Henceforth, when referring to the last synchronization event, we will drop the $[k-1]$ notation for simplicity.

These three parameters t_0, d_1, and d_2 are continuously being tracked by a local node to achieve synchronization. Using these parameters, it's possible to determine the local clock value of any event that is timestamped in the network clock.

According to the discrete noise propagation, the process noise affecting each of these parameters can be expressed in the following process noise matrix Q_t.

$$Q_t = \begin{bmatrix} \frac{\sigma_c^2}{20}dt^5 & \frac{\sigma_c^2}{8}dt^4 & \frac{\sigma_c^2}{6}dt^3 \\ \frac{\sigma_c^2}{8}dt^4 & \frac{\sigma_c^2}{3}dt^3 & \frac{\sigma_c^2}{2}dt^2 \\ \frac{\sigma_c^2}{6}dt^3 & \frac{\sigma_c^2}{2}dt^2 & \sigma_c^2\ dt \end{bmatrix} \tag{7}$$

$$[t, d_1, d_2]' \sim N(\mu, Q_t) \tag{8}$$

B. Timestamp measurements

The transmission timestamps are assumed to be from a perfect clock in this work. This assumption is reasonable as previous work of GCS [20], AGCS [11] have achieved synchronization accuracies in the order of tens of picoseconds, and the transmissions are timestamped in a stable network clock.

Assuming the synchronization is already obtained at the last transmission event tx_{k-1}, an estimate for the next transmission timestamp in local clock can be obtained using the propagation equations.

$$t_L[tx_k] = t_0 + d_1 dt + \frac{1}{2}d_2 dt^2 + \nu_t(dt) \tag{9}$$

Adding the time taken to travel the distance between the transmitter and the receiver r_k at the speed of light C, and the noise associated with a reception timestamp η_s, the local clock value at reception can be expressed as follows.

$$t_L[rx_k] = t_L[tx_k] + \frac{r_k}{C} + \eta_s \tag{10}$$

$$\hat{t_L}[rx_k] = (t_0 + d_1 dt + \frac{1}{2}d_2\, dt^2) + \frac{r_k}{C} \tag{11}$$

In contrast to this, a TDOA measurement used for comparison can be expressed as follows.

let Δr_k be the difference between r_k and r_{k-1}

$$\Delta r_k = r_k - r_{k-1} \tag{12}$$

$$\frac{\hat{\Delta r_k}}{C} = t_L[rx_k] - t_L[rx_{k-1}] - dt_N\, \dot{t}_L^N \tag{13}$$

C. Tightly coupled error state Kalman filter for localization

In order to estimate the 3D pose of a mobile platform, a localization Kalman filter usually keeps track of the position $\mathbf{p}$, velocity $\mathbf{v}$, orientation, and accelerometer and gyroscope biases $\mathbf{b_a}$, $\mathbf{b}_\omega$ as its states. In addition to these states, in our work, three states are included to precisely track the variations in the local clock of the UWB receiver. These added states are local clock phase t_0 and its first and second derivatives relative to the network clock d_1 and d_2. We have chosen velocity to be expressed in the world frame while the accelerometer and gyroscope biases are represented in the local frame for simplicity. With the quaternion $\mathbf{q}$ as the orientation parameterization, we denote the nominal states as follows.

$$\mathbf{x} = [\mathbf{p}^T, \mathbf{v}^T, \mathbf{q}^T, \mathbf{b_a}^T, \boldsymbol{b_\omega}^T, t_0, d_1, d_2]^T \tag{14}$$

Following the state definitions, nominal state dynamics can be derived as follows. Where η represents the noise parameters associated with each process.

$$\dot{\mathbf{x}} = f(\mathbf{x}, \mathbf{u}, \boldsymbol{\eta}) \tag{15}$$

$$\begin{bmatrix} \dot{\mathbf{p}} \\ \dot{\mathbf{v}} \\ \dot{\mathbf{q}} \\ \dot{\mathbf{b}}_\mathbf{a} \\ \dot{\mathbf{b}}_\omega \\ \dot{t}_0 \\ \dot{d}_1 \\ \dot{d}_2 \end{bmatrix} = \begin{bmatrix} \mathbf{v} \\ R(\mathbf{q})\,(\mathbf{a_m} - \mathbf{b_a} - \boldsymbol{\eta_a}) + \mathbf{g_e} \\ 0.5\Omega(\boldsymbol{\omega_m} - \boldsymbol{b_\omega} - \boldsymbol{\eta_\omega})\mathbf{q} \\ \boldsymbol{\eta_{ba}} \\ \boldsymbol{\eta_{b\omega}} \\ d_1 \\ d_2 \\ \eta_t \end{bmatrix} \tag{16}$$

Where Ω function expands as follows.

$$\Omega(w) = \begin{bmatrix} 1 & w \\ w^T & [w]_\times \end{bmatrix} \tag{17}$$

Gaussian noise driving the system can be encapsulated in the following process noise vector.

$$\boldsymbol{\eta} = [\boldsymbol{\eta}_a^T \ \ \boldsymbol{\eta}_\omega^T \ \ \boldsymbol{\eta}_{ba}^T \ \ \boldsymbol{\eta}_{b\omega}^T \ \ \eta_t]^T \tag{18}$$

The error states are defined as follows. Right definition of quaternion error was used here as it provides more consistent estimations [21].

$$\boldsymbol{\delta q} = \mathbf{q}\hat{\mathbf{q}}^{-1} = exp(\boldsymbol{\delta\theta}) \sim \begin{bmatrix} 1 \\ \boldsymbol{\delta\theta}/2 \end{bmatrix} \tag{19}$$

Here the $\boldsymbol{\delta\theta}$ represents the global perturbations in the orientation. Other error states are defined linearly, resulting the error state vector $\tilde{\mathbf{x}}$.

$$\delta x_i = x_i - \hat{x_i} \tag{20}$$

$$\tilde{\mathbf{x}} = \begin{bmatrix} \boldsymbol{\delta p}^T & \boldsymbol{\delta v}^T & \boldsymbol{\delta\theta}^T & \boldsymbol{\delta b_a}^T & \boldsymbol{\delta b_\omega}^T & \delta t_0 & \delta d_1 & \delta d_2 \end{bmatrix}^T \tag{21}$$

Error state dynamics can now be derived from nominal state dynamics and error state definitions.

$$\dot{\tilde{\mathbf{x}}} = \tilde{f}(\hat{\mathbf{x}}, \tilde{\mathbf{x}}, \mathbf{u}, \boldsymbol{\eta}) \tag{22}$$

$$\begin{bmatrix} \dot{\boldsymbol{\delta p}} \\ \dot{\boldsymbol{\delta v}} \\ \dot{\boldsymbol{\delta\theta}} \\ \dot{\boldsymbol{\delta b_a}} \\ \dot{\boldsymbol{\delta b}}_\omega \\ \dot{\boldsymbol{\delta t_0}} \\ \dot{\boldsymbol{\delta d_1}} \\ \dot{\boldsymbol{\delta d_2}} \end{bmatrix} = \begin{bmatrix} \boldsymbol{\delta v} \\ [R(\hat{\mathbf{q}})\,(\mathbf{a_m} - \hat{\mathbf{b_a}})]_\times \boldsymbol{\delta\theta} - R(\hat{\mathbf{q}})\boldsymbol{\delta b_a} - R(\hat{\mathbf{q}})\boldsymbol{\eta_a} \\ -R(\hat{\mathbf{q}})\boldsymbol{\delta b_\omega}) - R(\hat{\mathbf{q}})\boldsymbol{\eta_\omega} \\ \boldsymbol{\eta_{ba}} \\ \boldsymbol{\eta_{b\omega}} \\ d_1 \\ d_2 \\ \eta_t \end{bmatrix} \tag{23}$$

Following these dynamics, The discrete-time state propagation matrix can be derived as follows.

$$\begin{aligned} \boldsymbol{\Phi}_k =& I + dt\, \frac{\partial \tilde{\mathbf{f}}(\hat{\mathbf{x}}, \tilde{\mathbf{x}}, \mathbf{u}, 0)}{\partial \tilde{\mathbf{x}}}\bigg|_{\hat{\mathbf{x}}=\hat{\mathbf{x}}_k,\, \tilde{\mathbf{x}}=0} \\ =& \begin{bmatrix} I_{3\times3} & I_{3\times3}\,dt & 0_{3\times3} & 0_{3\times3} & 0_{3\times3} & 0_{3\times3} \\ 0_{3\times3} & I_{3\times3} & -[R\,at]_\times & -R\,dt & 0_{3\times3} & 0_{3\times3} \\ 0_{3\times3} & 0_{3\times3} & I_{3\times3} & 0_{3\times3} & -R\,dt & 0_{3\times3} \\ 0_{3\times3} & 0_{3\times3} & 0_{3\times3} & I_{3\times3} & 0_{3\times3} & 0_{3\times3} \\ 0_{3\times3} & 0_{3\times3} & 0_{3\times3} & 0_{3\times3} & I_{3\times3} & 0_{3\times3} \\ 0_{3\times3} & 0_{3\times3} & 0_{3\times3} & 0_{3\times3} & 0_{3\times3} & \phi t \end{bmatrix} \end{aligned} \tag{24}$$

Where,

$$\phi t = \begin{bmatrix} 1 & dt & 0.5dt^2 \\ 0 & 1 & dt \\ 0 & 0 & 1 \end{bmatrix} \tag{25}$$

The measurements for the filter are reception timestamps of the messages from stationary anchors and magnetometer readings. Accelerometer and gyroscope measurements are used as inputs to propagate the states.

$$\mathbf{y} = h(\hat{\mathbf{x}}, \tilde{\mathbf{x}}, \mathbf{u}, \boldsymbol{\nu}) \tag{26}$$

For n inbound messages, the measurement update matrix becomes.

$$\begin{aligned} \mathbf{H}_k =& \frac{\partial h(\mathbf{x}, 0, u, 0)}{\partial \tilde{\mathbf{x}}}\bigg|_{\mathbf{x}=\mathbf{x}_k^*} \\ =& \begin{bmatrix} 0_{3\times3} & 0_{3\times3} & [m_e]_\times & 0_{3\times6} & 0_{3\times3} \\ Hr & 0_{n\times3} & 0_{n\times3} & 0_{n\times6} & Ht \\ 0_{n\times3} & 0_{n\times3} & 0_{n\times3} & 0_{n\times6} & Hd \end{bmatrix} \end{aligned} \tag{27}$$

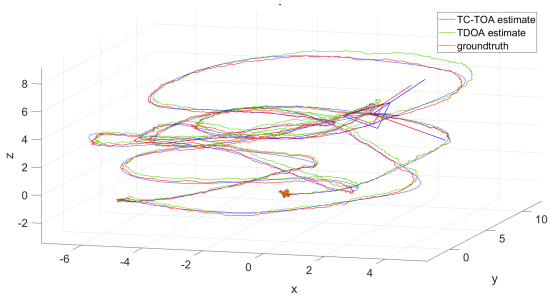

Fig. 2. Estimated path: simulations.

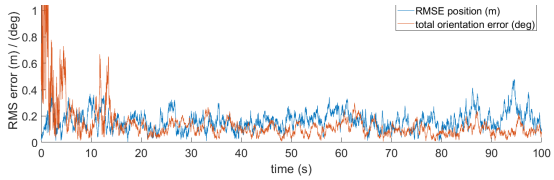

Fig. 3. RMSE position / total orientation error.

Where Hr correlates timestamp measurements with the position. Here $\mathbf{A_i}$ represents the coordinates of the anchor i.

$$Hr = \begin{bmatrix} \cdot \\ \frac{\mathbf{A_i}^T - \mathbf{p}^T}{\|\mathbf{A_i} - \mathbf{p}\|} \\ \cdot \end{bmatrix}_{n\times3} \tag{28}$$

Ht correlates timestamp measurements with clock dynamics,

$$Ht = \begin{bmatrix} \cdot & \cdot & \cdot \\ 1 & dt_i & 0.5dt_i^2 \\ \cdot & \cdot & \cdot \end{bmatrix}_{n\times3} \tag{29}$$

and Hd fuses clock offset ratio measurements.

$$Hd = \begin{bmatrix} 0_{n\times1} & 1_{n\times1} & 0_{n\times1} \end{bmatrix} \tag{30}$$

These equations, together with Standard Kalman filter update equations, were used to calculate the error state and update nominal states accordingly. More details on Kalman filter estimators can be found here [22]. Since the clock dynamics states t_0, d_1 and d_2 need to be propagated by accurate UWB network time, they are only propagated and corrected at the end of the network transmission cycle using the received transmission timestamps.

III. Simulation Results

The proposed EKF based estimator was evaluated on a simulation environment and compared with the TDOA method. A trajectory was generated using simulated inputs for body frame acceleration and angular rate. The clock dynamics were simulated following the third-order linear clock model. Equations introduced in [11] were used in

Case	Parameter	TC-TOA	TDOA
No anchor loss	RMSE position (m)	0.1585	0.2306
	total angle error(deg)	0.1432	0.1432
intermittent anchor loss downto 2 anchor	RMSE position (m)	0.1768	0.2463
	total angle error(deg)	0.1489	0.1432
intermittent anchor loss downto 1 anchor	RMSE position (m)	0.1782	0.2596
	total angle error(deg)	0.1489	0.1432

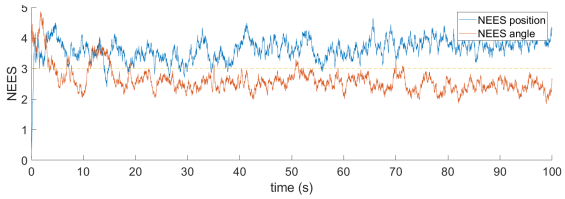

Fig. 4. NEES position, orientation TC-TOA.

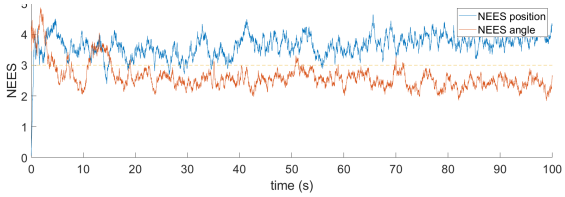

Fig. 5. NEES position, orientation TDOA.

the TDOA method while applying corrections for first-order clock dynamics.

Two sets of 100 Monte Carlo runs were repeated for both TC-TOA and TDOA methods, with identical noise figures for each set. TDOA method resulted around 21cm rms positioning errors, while the novel TC-TOA method resulted errors around 15cm. Furthermore, the proposed method showed improved consistency when the node moved away from the convex hull of anchors while the positioning error of TDOA method increased due to the geometric dilution of precision. The estimated path from the simulation is shown in Fig. 2.

To further evaluate the robustness of the proposed method, we considered two additional cases where the connection between the mobile node and the stationary anchors dropped intermittently. A similar scenario can be common on a low-density building-wide UWB network setup where having four or more anchors at the line of sight all the time can be impractical. In case 2, the connection was dropped down to 3 anchors for 2 seconds and down to 2 anchors for another 2 seconds. For 6 seconds, the mobile node received messages from all four nodes, and this pattern is set to repeat after 10 seconds. for case 3, the connection was

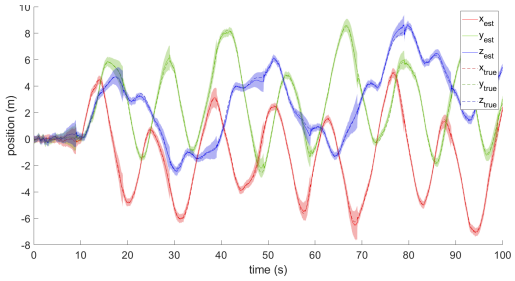

Fig. 6. Estimated coordinates: simulation.

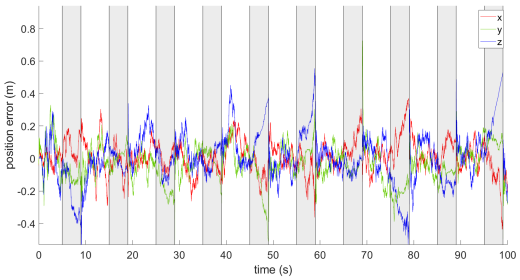

Fig. 7. Position estimation error.

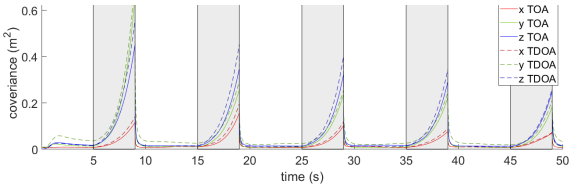

Fig. 8. Position estimation covariance.

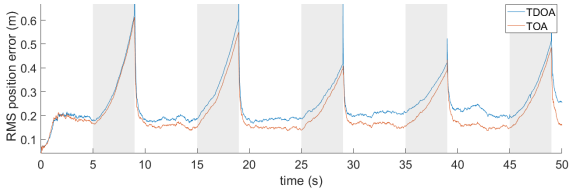

Fig. 9. RMSE position.

only dropped down to 2 and 1 anchors, following the same pattern. The performance was compared with the traditional TDOA measurement update. It could be clearly seen that the tightly coupled measurement update resulted Superior positioning accuracy in all the cases tested. The reduced drift in the estimations as well as lower estimation covariance values during these un-observable cases, indicate improved consistency over the TDOA method.

It is worth mentioning that when the mobile node is receiving messages only from a single anchor, the TDOA method cannot apply a measurement correction. Yet the proposed tightly coupled method can apply a measurement correction as it keeps track of the network clock phase.

IV. Experimental Validation

The proposed filter was evaluated offline with a captured data set using a UWB receiver attached to a DJI quadcopter. The data collection hardware includes a DWM1001-DEV

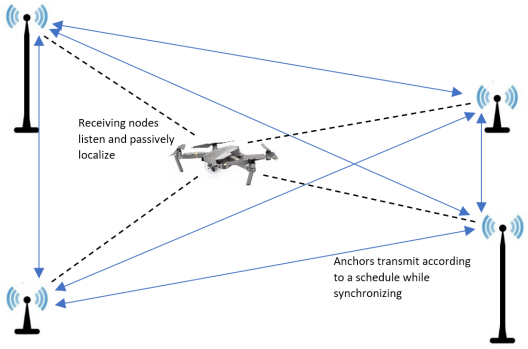

Fig. 10. Experimental setup.

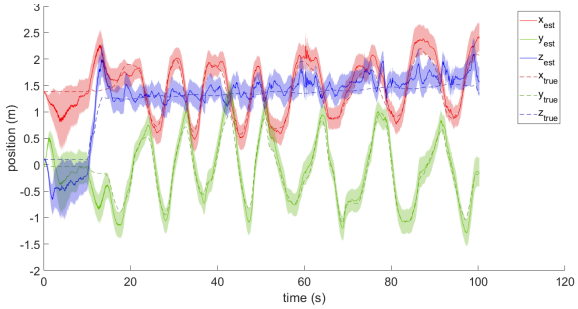

Fig. 11. TC-TOA position estimation.

UWB transceiver board and an MTI-1 series IMU. The quadcopter was flown manually under the observation of a motion capture system while receiving messages from the UWB localization network. AGCS framework [11] is used in network synchronization, resulting RMS network synchronization errors around 45ps. IMU and magnetometer data was logged at 100Hz, while UWB messages were received at around 15ms apart.

Observed reception timestamp measurements were used to update the Kalman filter after initializing with the ground truth from the motion capture system. For simulated intermittent connection loss, measurement updates from some of the anchors were skipped for a 2s duration, repeating every 10s. For comparison, the same dataset was used with the TDOA method.

Case	Parameter	TC-TOA	TDOA
no anchor loss	RMSE position (m)	0.247	0.258
	total angle error (deg)	2.23	9.11
intermittent anchor loss for 2s	RMSE position (m)	0.293	0.319
	total angle error (deg)	2.17	9.05

Results show that the proposed TC-TOA method has an improved positioning accuracy when compared to the TDOA method. For the compared TDOA method, relative clock rate estimate from a decoupled Kalman filter is used, which gives the best estimate without incorporating coupled dynamics. Fig. 11 shows the estimated position coordinates together with the ground truth from the motion capture system. Three sigma bounds for the estimation confidence are shown in shaded regions. It can be seen that the ground truth lies within these bounds most of the time. For 3D localization without anchor loss, RMS position errors were found to be 0.25m. These figures are comparable to values found in similar TDOA systems [10], but should not be directly compared as the systems have differences in the number of anchors, processing hardware, and the update rate.

V. Discussion and conclusion

This paper presented a novel passive localization solution for Ultra-wideband ranging networks based on tightly coupled dynamics and an error state Kalman filter. The time of arrival measurements are used in updating the filter. Magnetometer measurements are used as an additional orientation measurement. The results show that the tightly coupled system gives superior positioning accuracy than the traditional TDOA system. The novel method has shown improved consistency as well as higher robustness against momentary loss of connection with anchors. The proposed method also can perform measurement updates even when receiving messages from one anchor, while the TDOA method requires a minimum of two anchors to perform a measurement update.

The extended work will target analyzing and comparing both TDOA and TC-TOA methods at different transmission gaps, incorporating the correlations between timestamp measurements as well as an optimization-based solution for the tightly coupled system.

References

[1] C. Almansa, W. Shule, J. P. Queralta, and T. Westerlund, "Autocalibration of a uwb localization system for dynamic and ad-hoc deployments in gnss-denied environments," *ArXiv*, vol. abs/2004.06762, 2020.

[2] T.-M. Nguyen, M. Cao, S. Yuan, Y. Lyu, T. H. Nguyen, and L. Xie, "Viral-fusion: A visual-inertial-ranging-lidar sensor fusion approach," *IEEE Transactions on Robotics*, vol. 38, pp. 958–977, 2020.

[3] M. Kwak and J. Chong, "A new double two-way ranging algorithm for ranging system," in *2010 2nd IEEE InternationalConference on Network Infrastructure and Digital Content*, pp. 470–473, IEEE, 2010.

[4] Y. Jiang and V. C. Leung, "An asymmetric double sided two-way ranging for crystal offset," in *2007 International Symposium on Signals, Systems and Electronics*, pp. 525–528, IEEE, 2007.

[5] G.-C. Pătru, L. Flueratoru, I. Vasilescu, D. Niculescu, and D. Rosner, "Flextdoa: Robust and scalable time-difference of arrival localization using ultra-wideband devices," *IEEE Access*, vol. 11, pp. 28610–28627, 2023.

[6] J. Wang, R. Ghosh, and S. Das, "A survey on sensor localization," *Journal of Control Theory and Applications*, vol. 8, pp. 2–11, 02 2010.

[7] B. Xu, G. Sun, R. Yu, and Z. Yang, "High-accuracy tdoa-based localization without time synchronization," *IEEE Transactions on Parallel and Distributed Systems*, vol. 24, no. 8, pp. 1567–1576, 2013.

[8] J. Tiemann, F. Eckermann, and C. Wietfeld, "Multi-user interference and wireless clock synchronization in tdoa-based uwb localization," in *2016 International Conference on Indoor Positioning and Indoor Navigation (IPIN)*, pp. 1–6, 2016.

[9] J. Tiemann and C. Wietfeld, "Scalable and precise multi-uav indoor navigation using tdoa-based uwb localization," in *2017 International Conference on Indoor Positioning and Indoor Navigation (IPIN)*, pp. 1–7, 2017.

[10] M. Hamer and R. D'Andrea, "Self-calibrating ultra-wideband network supporting multi-robot localization," *IEEE Access*, vol. 6, pp. 22292–22304, 2018.

[11] N. M. Senevirathna, O. De Silva, G. K. I. Mann, and R. G. Gosine, "Asymptotic gradient clock synchronization in wireless sensor networks for uwb localization," *IEEE Sensors Journal*, vol. 22, no. 24, pp. 24578–24592, 2022.

[12] S. Godha and M. E. Cannon, "Gps/mems ins integrated system for navigation in urban areas," *GPS Solutions*, vol. 11, no. 3, p. 193–203, 2007.

[13] G. Falco, M. Pini, and G. Marucco, "Loose and tight gnss/ins integrations: Comparison of performance assessed in real urban scenarios," *Sensors*, vol. 2017, p. 27, 01 2017.

[14] M. Petovello, C. O'Driscoll, and G. Lachapelle, "Ultra-tight gps/ins for carrier phase positioning in weak signal environment," 01 2007.

[15] H.-S. Kim, S.-C. Bu, G.-I. Jee, and C. Park, "An ultra-tightly coupled gps/ins integration using federated kalman filter," 01 2003.

[16] J. A. Corrales Ramon, F. Candelas Herias, and F. Torres, "Sensor data integration for indoor human tracking," *Robotics and Autonomous Systems*, vol. 58, pp. 931–939, 08 2010.

[17] W. Jiang, Z. Cao, B. Cai, B. Li, and J. Wang, "Indoor and outdoor seamless positioning method using uwb enhanced multi-sensor tightly-coupled integration," *IEEE Transactions on Vehicular Technology*, vol. 70, no. 10, pp. 10633–10645, 2021.

[18] Y. Xu, Y. S. Shmaliy, C. K. Ahn, T. Shen, and Y. Zhuang, "Tightly coupled integration of ins and uwb using fixed-lag extended ufir smoothing for quadrotor localization," *IEEE Internet of Things Journal*, vol. 8, no. 3, pp. 1716–1727, 2021.

[19] Z. Liu, J. Li, A. Wang, X. Cheng, and A. Wang, "Design and implementation of uwb/mimu tightly-coupled system for indoor positioning," in *2018 Ubiquitous Positioning, Indoor Navigation and Location-Based Services (UPINLBS)*, pp. 1–7, 2018.

[20] P. Sommer and R. Wattenhofer, "Gradient clock synchronization in wireless sensor networks," in *2009 International Conference on Information Processing in Sensor Networks*, pp. 37–48, IEEE, 2009.

[21] R. G. Thalagala, O. De Silva, G. K. I. Mann, and R. G. Gosine, "Efficient and Consistent Two Key-Frame Visual-Inertial Navigation Using Matrix Lie Groups," *Journal of Dynamic Systems, Measurement, and Control*, vol. 145, p. 011001, 10 2022.

[22] R. Faragher, "Understanding the basis of the kalman filter via a simple and intuitive derivation [lecture notes]," *IEEE Signal processing magazine*, vol. 29, no. 5, pp. 128–132, 2012.